The caudate nucleus contributes causally to decisions that combine noisy visual evidence and reward context

Takahiro Doi[1,3], Yunshu Fan[1,2], Joshua I. Gold[1,2], Long Ding[1,2]*

[1]Department of Neuroscience, University of Pennsylvania, Philadelphia, PA 19104

[2]Neuroscience Graduate Group, University of Pennsylvania, Philadelphia, PA 19104

[3]Department of Psychology, University of Pennsylvania, Philadelphia, PA 19104

Corresponding author: Long Ding

Abstract

Decision making is a complex process that interprets sensory information within the context of non-sensory factors such as reward expectation. How this process is implemented in the brain remains unclear. Here we show that, in monkeys making decisions based on noisy visual evidence and asymmetric reward context, neuronal activity in the caudate nucleus varies with evidence strength and reward context during decision formation, at both the population and single-neuron levels. Electrical microstimulation during motion viewing also induced changes in decision behavior that depended on neural activity patterns at the stimulation site. Within a drift-diffusion framework, distinct correlation patterns of the microstimulation effects on multiple parameters suggest that caudate neurons transform reward context information into a common signal to coordinate adjustments in decision-related computations and participate more directly to implement decision bound- and evidence accumulation-related computations. These results establish a central, causal role of the caudate nucleus in complex decision decision-making.

Keywords: basal ganglia, caudate, perceptual decision, reward, saccade, drift diffusion, electrophysiology, non-human primate, oculomotor

Acknowledgments We thank Jean Zweigle for animal care. This work was supported by NIH National Eye Institute (R01-EY022411) (L.D. and J.I.G), University of Pennsylvania (University Research Foundation Pilot Award) (L.D.), and Hearst Foundations Graduate student fellowship (Y.F.).

Author contributions: Conceptualization, L.D. and J.I.G.; Methodology, Investigation, all authors; Software Visualization and Writing – Original Draft, L.D; Writing – Review and Editing, all authors.; Supervision and Project Administration, L.D.; Funding Acquisition, L.D. and J.I.G.

The authors declare no competing interests

The basal ganglia have been proposed to perform general selection-related computations, including for value-based decisions that focus on expected outcome and for perceptual decisions that depend on sensory evidence [1-14]. Neurons in the basal ganglia show decision formation-related activity during both reward-based and perceptual decision tasks and perturbation of these activity causally influences decision performance [15-27]. These results led to the conjecture that the basal ganglia may play strategic roles in complex decisions that require incorporation of sensory evidence and reward expectation [2, 28].

To test this conjecture, we targeted the caudate nucleus, an input station in the oculomotor basal ganglia pathway. We trained monkeys to report their perceived motion direction of a random-dot kinematogram at a self-determined time (Fig. 1)[29]. We manipulated motion strength across trials and reward-choice association across blocks of trials. The monkeys' performance showed clear dependence on visual motion evidence and reward asymmetry (Fig. 1b).

We recorded single-unit activity from 142 neurons (n = 49 for monkey C and 93 for monkey F) and found that many neurons showed joint modulation by both reward and evidence strength. The example neuron in Fig. 1c showed three types of modulation: it was more active for trials with contralateral choice, both during motion viewing and around saccade onset (Contra > IPSI), more active during the blocks when the contralateral choice was paired with small reward and the ipsilateral choice was paired with large reward (green > purple), and more active for trials with higher coherence levels, particularly for trials with contralateral choices (dark shade> light shade). Across the population, caudate neurons showed diverse patterns of modulation by choice, reward context, expected reward size, and motion strength, as measured using multiple linear regression analysis (Extended Data Fig. 1). At the population level, the representation of reward context emerged before motion stimulus onset and persisted throughout the trial, while other quantities were reflected in the activity of gradually increasing numbers of neurons during motion viewing.

At the single-neuron level, we defined reward modulation as significant regression coefficients for either reward context or reward size, visual evidence modulation as significant coefficients for coherence for either choices, and combination modulation as both reward and visual evidence modulations. We found 101 neurons showing combination modulation in at least one task epochs (Fig. 1d). We focused on the 50 neurons showing combination modulation during motion viewing. During this deliberation period, the actual modulation patterns varied considerably among combination neurons (Fig. 1e), with three notable features: 1) there was a contralateral dominance in choice preference, as represented by the high yellow : dark-blue ratio in the first row [21]; 2) when significant coherence modulation was observed for both choices, the modulation were of the same sign for both choices (Fig. 1f, blue circles), consistent with reflecting a coherence-dependent evaluative signal; and 3) the signs of choice and reward context modulation were the same only for some, but not all, neurons (Fig. 1g). For example, the neuron in Fig. 1c was more active for contralateral-choice trials and for ipsilateral-large reward blocks.

The presence of combination neurons suggests that the caudate nucleus may contribute to the incorporation of visual evidence and reward information. To test for such a causal contribution, in 55 sessions, we first identified a caudate site with task-related activity and then interleaved trials with and without microstimulation at 1:1 ratio (n = 24 sessions for monkey C and 31 for monkey F). We observed microstimulation-induced choice biases in many sessions. In the example session shown in Fig. 2a, for trials without microstimulation, the monkey showed a reward bias favoring the large reward (black solid line was to the left of the black dashed line). With microstimulation, both curves were shifted to the left (red lines), suggesting that microstimulation at this caudate site induced bias favoring the rightward choice in both reward contexts and with similar magnitude. In many other sessions, however, microstimulation induced choice biases differently for the two reward contexts. Fig. 2b shows an example session in which microstimulation induced a rightward choice bias when the large reward was paired with the rightward choice (the red solid line is to the left of the black solid line) and a leftward choice bias when the large reward was paired with the leftward choice (the red dashed line is to the right of the black dashed line). That is, microstimulation at this caudate site enhanced the reward bias. Fig. 2c shows another example session in which microstimulation enhanced the reward bias, by inducing a much larger leftward choice bias when the leftward choice was paired with large reward.

To quantify these effects, we fitted the choice data for each session to a logistic function that contained bias and sensitivity terms that depended on reward context, microstimulation status, or their interactions. Across the sessions, microstimulation induced an overall contralateral choice bias (Fig. 2d, top histogram) and a reward context-dependent choice bias favoring the contralateral choice when it was paired with large reward (right histogram). Microstimulation also induced an overall reduction in sensitivity (Fig. 2e, top histogram) and a larger reduction when the contralateral choice was paired with large reward reduction (right histogram). A different representation of these results, which contrasts microstimulation effects between reward contexts, is shown in Extended Data Fig. 2a and b. These results showed that caudate microstimulation induced both reward context-independent and -dependent changes in monkey's choice bias and sensitivity, suggesting a causal link between caudate activity and decision formation that depended on reward information and visual evidence.

To understand better the computations that underlie the causal link, we analyzed the choice and single-trial RT data within a drift-diffusion framework (DDM; Fig. 3a). We used model selection procedures to identify sessions with significant modulation of DDM parameters and to identify critical parameters in those sessions. By comparing the AIC values between a full model, in which all parameters were allowed to vary with microstimulation, and a reduced model in which all parameters were fixed, we identified 39 sessions that showed significant microstimulation effect on at least one DDM parameter (Extended Data Fig. 2c). By comparing AIC values among the full model and reduced models in which one parameter was fixed, we found that parameters related to the temporal dynamics of the decision bounds were not critical, but omitting other

DDM parameters (*a*, *k*, *me*, *z* and non-decision times *t0*) impaired the goodness-of-fit for most sessions (Fig. 3b). Closer examination of the best-fitted values for these latter parameters revealed complex patterns (Extended Data Fig 3). In a reward context-independent manner, microstimulation reduced decision bound (*a*) and the scaling factor for evidence (*k*), increased non-decision times for both choices, and had variable effects on the fictive evidence (*me*) and relative bound heights (*z*) (top row). In a reward context-dependent manner, microstimulation reduced *k* further when the contralateral choice was paired with large reward and had variable effects on other parameters (bottom row). Note that, because choice bias was controlled by both *me* and *z*, variable but correlated changes in *me* and *z* can still generate consistent changes in biasvv. These results suggest that caudate microstimulation altered monkeys' decision performance by changing the processes that control multiple DDM parameters.

The multi-faceted and variable nature of the microstimulation effects led us to hypothesize that the effects for a given session may depend on which neurons were perturbed at the stimulation site and/or unknown constraints on the caudate neurons' general roles in the decision process. To test the former, we examined the relationship between modulation patterns of neural activity and the microstimulation effects. First, as expected from the heterogeneity shown above, we did not detect any obvious relationship between a particular type of microstimulation effect and modulation pattern of neural activity, measured as regression coefficients for choice, reward context, reward size, coherence and reward-coherence interactions (Extended Data Fig. 4). For example, activity at site "a" showed significant modulation by choice, reward context, reward size and reward-coherence interaction, the microstimulation induced a reward context-independent choice bias (example in Fig. 2a). Activities at sites "b" and "c" showed simpler modulation patterns, but microstimulation induced strong reward context-dependent biases, with additional differences in signs between the two sites (examples in Fig. 2b and c).

On the other hand, we observed significant dependence of the magnitude of certain microstimulation effects on the strength of neural modulation. Specifically, we focused on three hypothesized relationships. First, the reward context-modulated caudate activity has been proposed to bias choice behavior [2, 30, 31], by providing a non-zero starting value (*z*) for the accumulation process to bias toward the preferred, large-reward choice. We observed a positive correlation between the choice selectivity of the units at the stimulation site and the reward context-independent microstimulation effect on *z* (Fig. 3c; black, $p = 0.018$). Closer examination revealed that such a correlation was only present if the units showed congruent choice and reward context modulation (e.g., higher activity for the contralateral choice and when the contralateral choice was paired with large reward) (Fig. 3c; red, $p = 0.026$; $p = 0.72$ for incongruent preferences). Second, if caudate neurons contribute to evidence accumulation to support either decision formation or evaluation, perturbation of neurons sensitive to motion strength may affect the effective scaling factor for evidence (*k*). We found a positive correlation between the strength of coherence modulation and reward context-independent microstimulation effect on *k*, but only if the neurons showed the same sign in coherence modulation for both

choices (Fig. 4d and e; $p = 0.023$ and 0.009 for sites with the same sign; $p > 0.4$ for sites with opposite signs). Lastly, we hypothesized that neurons sensitivity to reward context or expected reward size may contribute to the reward context-dependent microstimulation effects. We observed a negative correlation between reward size modulation and reward context-dependent microstimulation effect on choice bias (Fig. 4f; $p = 0.027$; i.e., perturbation of sites with large reward-preferring activity reduced the reward asymmetry-induced bias). This relationship was not reflected in changes in either *me* or *z* (Extended Data Fig. 5a and b). The same tendencies were found in both monkeys (Extended Data Fig. 6). We did not observe any dependence of microstimulation effects on neurons' reward context modulation (Extended Data Fig. 5c). These results suggest that the heterogeneity in microstimulation effects reflected the heterogeneity in the perturbed caudate neurons' roles in decision formation.

We next examined the patterns of reward asymmetry-induced changes in DDM parameters and their similarity with microstimulation effects, to infer the general roles of caudate neurons in the context of reward-biased decision-making (Extended Data Fig. 7a-d). In monkeys performing this task, *me* and *z* were adjusted in sensitivity-dependent ways to favor small- and large-reward choices, respectively [29], resulting in a negative correlation between their reward asymmetry-induced changes (Fig. 4a). Strikingly, a nearly identical negative correlation was present in their reward context-dependent microstimulation effects (Fig. 4b). This correlation was absent in their reward context-independent microstimulation effects (Fig. 4c), arguing against an artificial relationship (e.g., from model fitting) and, instead, supporting the idea that the perturbed neurons were part of the reward context-processing circuit that provides a common modulatory signal to adjust *me* and *z* by other neurons. Among the DDM parameters, correlation patterns present in reward asymmetry-induced adjustments were preserved in reward context-dependent microstimulation effects, while only a subset of these correlations were present in reward context-independent microstimulation effects (Fig. 4d; Extended Data Figs. 7e-g and 8-10 for correlation patterns for individual monkeys and raw scatterplots). Notably, the reward context-independent microstimulation effects on *a* and *k* were not correlated with any other parameters, suggesting that the perturbed neurons play a more direct role in their adjustments. Principal component analysis further confirmed these intuitions. Fig 4e visualizes the 3-dimensional space defined by principal components derived from the "rew" effects on DDM parameters and the projections of "rew", "rew x estim" and "estim" effects in this space. The "rew x estim" cluster (purple) was tighter and more similarly oriented as the "rew" cluster (red) than the "estim" cluster (green). This difference was also apparent in the cumulative fraction of explained variance using PCs derived from "rew" data, which was higher for "rew x estim' than "estim" (Fig. 4f). These results suggest that microstimulation had two consequences (Fig. 4g): it perturbed a common process that coordinates reward asymmetry effects for DDM parameters; it also perturbed separate processes that directly control *a* and *k*.

Collectively, our results suggest that caudate neurons causally contribute to decision-making that requires incorporation of reward asymmetry information and visual evidence. Their contributions

likely include transforming reward asymmetry into a common modulatory signal to coordinate adjustments in decision-related computations and participating more directly to implement decision bound and to evidence weight- related computations [4].

Methods

We used two male rhesus macaques (*Macaca mulatta*) for this study. As described before [29], they had been first trained extensively on an equal-reward reaction-time random-dot motion discrimination task [21, 22, 32] and then trained with the asymmetric-reward contexts. All training and experimental procedures were in accordance with the National Institutes of Health Guide for the Care and Use of Laboratory Animals and were approved by the University of Pennsylvania Institutional Animal Care and Use Committee.

Behavioral task

Task details have been reported in a previous publication [29]. Briefly, a trial began with a central fixation point presentation. Upon acquiring and maintaining fixation, two choice targets were presented to inform the monkeys the two possible motion directions. After a random delay picked from a truncated exponential distribution (mean = 0.7 s, range: 0.4~2.5 s), the fixation point was dimmed and a random-dot kinematogram was shown at the center of the screen ("dots onset"). For each trial, the kinematogram had a constant speed of 6 °/s, aperture size of 5°, and randomly interleaved motion direction and strength (5 levels of %coherence: 3.2, 6.4, 12.8, 25.6, 51.2). The monkey reported the perceived motion direction by making a self-timed saccade to the corresponding choice target. A minimum 50-ms latency was imposed, although the monkeys rarely made fast-guess responses during this study. Once the monkey's gaze left the fixation window (4° square window), the kinematogram was extinguished. Once the monkey's gaze reached the choice target window (4° square window), a 400-ms minimum fixation time was imposed to register the monkey's choice. Correct choices were rewarded with juice. Error choices were not rewarded and penalized with a timeout before the next trial (3 s for monkey F, 0.5-2 s for monkey C).

Two asymmetric reward contexts were alternated in a block design. In Contra-LR blocks, the choice contralateral to the recording/stimulation site was paired with large reward. In Ipsi-LR blocks, the choice ipsilateral to the recording/stimulation site was paired with large reward. The other choice was paired with small reward. At the start of each block, the choice targets were presented with different colors to signal the current reward context to the monkeys, followed by two additional high-coherence trials to allow the monkeys to physically experience the current reward context. These trials were excluded from analysis.

Data acquisition

Eye position was monitored using a video-based system (ASL) sampled at 240 Hz. RT was measured as the time from stimulus onset to saccade onset, the latter identified offline with respect to velocity (> 40°/s) and acceleration (> 8000°/s2). Single-unit recordings were

performed as described previously, with a focus on putative project neurons [21]. We searched for task-relevant neurons while the monkeys performed the equal-reward motion discrimination task with horizontal dots motions and determined the presence of task-related modulation of neural activity by visual and audio inspection of ~10-20 trials. For the dataset used for characterizing joint modulation by reward and evidence, only single-unit recordings were included. For the dataset used for examining the microstimulation effects, sites with either single-unit or multi-unit task-related modulations were used. Neural signals were amplified, filtered and stored using a MAP acquisition system (Plexon, Inc.), along with time-stamped event codes, analog eye position signals and strobed trial parameter values. Single unit activity was identified by offline spike sorting (Offline Sorter, Plexon, Inc.). Multiunit activity was measured using waveforms that passed an offline amplitude threshold. Electrical microstimulation was delivered during motion stimulus presentation (negative-leading bipolar current pulses, 300 Hz, 50 µA, 250 µs pulse duration) in half of trials randomly interleaves with no-stimulation trials. As reported previously, caudate microstimulation with these parameters do not evoke saccades [22, 33-35].

Neural data analysis

For each single/multi-unit dataset, we computed the average firing rates in 7 task epochs. These included three epochs before motion stimulus onset (400 ms window beginning at target onset, variable window from target onset to dots onset, and 400 ms window ending at dots onset), two epochs during motion viewing (a fixed window from 100 ms after dots onset to 100 ms before median RT and a variable window from 100 ms after dots onset to 100 ms before saccade onset), a peri-saccade 300 ms window beginning at 100 ms before saccade onset, and a post-saccade 400 ms window beginning at saccade onset (before reward delivery). For each unit, a multiple linear regression was performed on each task epoch separately.

$$FR = \beta_0 + \beta_{Choice} \times I_{Choice} + \beta_{RewCont} \times I_{RewCont} + \beta_{RewSize} \times I_{RewSize}$$

$$+ \beta_{Coh-Contra} \times I_{Coh-Contra} + + \beta_{Coh-IPSI} \times I_{Coh-IPSI}$$

$$+ \beta_{RewCoh-Contra} \times\times I_{Coh-Contra} \times I_{RewSize} + \beta_{RewCoh-IPSI} \times\times I_{Coh-IPSI} \times I_{RewSize},$$

where $I_{Choice} = \begin{cases} 1\ for\ contralateral\ choice \\ -1\ for\ ipsilateral\ choice \end{cases}$,

$I_{RewCont} = \begin{cases} 1\ for\ contralateral - large\ Reward \\ -1\ for\ ipsilateral - large\ Rew \end{cases}$,

$I_{RewSize} = \begin{cases} 1\ for\ large\ reward \\ -1\ for\ small\ reward \end{cases}$,

$I_{Coh-Contra} = \begin{cases} absolute\ coherence\ for\ contralateral\ choice\ (centered\ at\ mean\ value) \\ 0\ for\ ipsilateral\ choice \end{cases}$,

and $I_{Coh-IPSI} = \begin{cases} 0\ for\ contralateral\ choice \\ absolute\ coherence\ for\ ipsilateral\ choice\ (centered\ at\ mean\ value) \end{cases}$.

Significance of non-zero coefficients was tested using *t*-test (criterion: $p = 0.05$). The number of units showing non-zero coefficients for each epoch was tallied and compared to the chance level (Fig. 1d and Extended Data Fig. 1).

For the microstimulation experiments, we recorded single- or multi-unit activity before microstimulation and performed multiple linear regression as above for each unit separately and normalized the regression coefficients to β_0. If more than one unit was recorded, for each regressor, we used the unit with the lowest *p* value.

Behavioral analysis

For each microstimulation session, a logistic function was fitted to the choice data for all trials:

$$P_{contra\ choice} = \frac{1}{1+e^{-Sensitivity \times (Coh-Bias)}} \quad ,$$

where $Sensitivity = s0 + s_{rew} \cdot RewCont + s_{estim} \cdot Estim + s_{rew \times estim} \cdot RewCont \cdot Estim$,
$Bias = bias0 + bias_{rew} \cdot RewCont + bias_{estim} \cdot Estim + bias_{rew \times estim} \cdot RewCont \cdot Estim$,

$$RewCont = \begin{cases} 1\ for\ contralateral - large\ Reward \\ -1\ for\ ipsilateral - large\ Rew \end{cases} ,$$

and $Estim = \begin{cases} 1\ for\ microstimulation\ trials \\ 0\ for\ control\ trials \end{cases}$.

We fitted the choice and RT data to different variants of the drift-diffusion model (DDM; Fig. 2f). The basic DDM assumed that the decision variable (DV) is the time integral of evidence (E), which was modeled as a Gaussian distributed random variable,

$$E \sim N(k * coherence, 1) \qquad \text{and} \qquad DV = \int E\, dt$$

The scaler *k* controlled the drift rate. At each time point, the DV was compared with two collapsing choice bounds [36]. The time course of the choice bounds was specified as $a/(1 + e^{\beta_alpha(t-\beta_d)})$, where β_alpha and β_d controlled the rate and onset of decay, respectively. If DV crossed the upper bound first, a contralateral choice was made; if DV crossed the lower bound first, an ipsilateral choice was made. RT was modeled as the sum of the time till first bound crossing and saccade-specific non-decision times that accounted for evidence-independent sensory/motor delays. Two types of biases were used to account for reward asymmetry-induced biases, a bias in drift rate (*me*) and a bias in the starting point (*z*)[29].

DDM model fitting was performed, separately for each session, using the maximum *a posteriori* estimate method (python v3.5.1, pymc 2.3.6). We performed at least 5 runs for each variant and used the run with the highest likelihood for further analyses. As a sanity check for the quality of fits, we compared the perceptual sensitivity and choice bias estimated from logistic function fits to those estimated using the “NoCollapse” variant. Both perceptual sensitivity and choice bias

were highly correlated between these two estimation methods (correlation coefficients = 0.85 and 0.98, respectively; p < 1e-50 for both). For a given DDM parameter, we parsed the different effects as follows (LR: large reward):

$$Para(base) = (Para_{contral-LR,no\ estim} + Para_{Ipsi-LR,no\ estim})/2$$

$$Para(rew) = (Para_{contral-LR,no\ estim} - Para_{Ipsi-LR,no\ estim})/2$$

$$Para(estim) = (Para_{contral-LR,estim} + Para_{Ipsi-LR,estim} - Para_{contral-LR,no\ estim} - Para_{Ipsi-LR,no\ estim})/2$$

$$Para(rew \times estim) = (Para_{contral-LR,estim} - Para_{Ipsi-LR,estim} - Para_{contral-LR,no\ estim} + Para_{Ipsi-LR,no\ estim})/2$$

Principal component analysis (PCA) was performed using python scikit-learn v0.18.1. Before PCA, the DDM parameters were pooled across “rew”, “rew x estim” and “estim” measurements to find the range for each parameter. The DDM parameters were then normalized linearly to these ranges such that each normalized parameter was in the range of [0, 1].

Figure Legends

Figure 1. Task, behavior and caudate activity.

a) On the asymmetric reward motion discrimination task, a monkey observed the random-dot motion stimulus and reported the perceived global motion with a saccade to one of the two choice targets. Motion direction and strength (coherence) were pseudo-randomly selected from trial to trial. In a block of trials, correct rightward choice was paired with large reward and correct leftward choice was paired with small reward. Error trials were not rewarded. The asymmetric reward contexts were alternated between blocks of trials.

b) Average choice behavior of two monkeys (n = 17493 trials from 38 sessions for monkey C and 29599 trials from 79 sessions for monkey F). Note the gap between red and blue curves, which indicates that both monkeys were more likely to choose the choice paired with large reward.

c) Example neuron showing joint modulation by choice, motion strength and reward context. Colors indicate reward contexts; shading indicates the coherence level.

d) Percentage of neurons showing joint visual evidence and reward modulation. Dashed line indicates chance level.

e) Color map showing the presence of significant non-zero regression coefficients for each combination neuron (in rows). Yellow: positive; dark blue: negative; green: not significant; criterion: $p = 0.05$. Neurons were sorted by the signs of coefficients.

f) Scatterplot of regression coefficients for coherence for the two choices. Only combination neurons with significant choice selectivity were shown. Gray: neurons without significant coherence modulation; cyan: neurons with significant coherence modulation for only one choice; red: neurons with significant coherence modulation for both choices.

g) Scatterplot of regression coefficients for choice and reward context for combinations neurons with significant modulation by either during motion viewing. Cyan: neurons with significant modulation by either choice or reward context; red: neurons with significant modulation by both.

Figure 2. Caudate microstimulation affected monkeys' decision behavior.

a-c) Three example sessions from monkey C, showing different patterns of microstimulation effects.

d) Scatterplot of the fitted $bias_{estim}$ and $bias_{rew\times estim}$ terms in logistic function. Top panel: histogram of the fitted $bias_{estim}$ term (median 0.79% coherence, Wilcoxon signed rank test, $p = 0.015$). Right panel: histogram of the fitted $bias_{rew\times estim}$ term (median 0.83% coherence, $p = 0.0035$). Colored circles with labels (a, b, c) correspond to the example sessions in a-c.

e) Scatterplot of the fitted s_{estim} and $s_{rew\times estim}$ terms in logistic function. Top panel: histogram of the fitted s_{estim} term (median -2.1, $p = 0.0012$). Right panel: histogram of the fitted $s_{rew\times estim}$ term (median -1.8, , $p = 0.019$). Colored circles with labels (a, b, c) correspond to the example sessions in a-c.

Figure 3. Microstimulation effects depended on neural modulation strength.

a) Drift-diffusion model. Motion evidence (E) is modeled as samples from a Gaussian distribution (mean = $k\times$ *signed coh*, var = 1). Decision variable is computed as the time integral of E and compared at each time point to two time-varying decision bounds. Crossing of either bound results in the corresponding choice. Reaction time is modeled as the sum of the time to bound-crossing and a non-decision time. See Methods for details.

b) Color map showing the best DDM variant for sessions with microstimulation effects, which was defined as showing a smaller AIC with the full model than a reduced model without microstimulation-induced changes (sessions to the left of the red arrow in Extended Data Fig. 2c).

c) Scatterplot of the regression coefficient value for "Choice" and the reward context-independent microstimulation effect on z. Black circles and line: all sessions. Red circles and line: sessions in which the choice and reward context preferences were congruent.

d-e) Scatterplot of the regression coefficient value for coherence for trials with contralateral (d) and ipsilateral choices (e) and the reward context-independent microstimulation effect on k. Black circles: all sessions. Red circles and line: sessions in which the two coefficients for Coh-Contra and Coh-IPSI had the same signs.

f) Scatterplot of the regression coefficient value for RewSize and the reward context-dependent microstimulation effect on choice bias. Only sessions with significant microstimulation effects on choice bias (for either reward context) was included.

Figure 4. Correlated microstimulation effects on DDM parameters reflected correlated reward asymmetry effects.

a) Scatterplot of reward context modulation of *me* and z in the absence of microstimulation. The solid line indicates linear regression results with a significant, non-zero slope value. Shaded area indicates 95% confidence interval.

b) Scatterplot of reward context-dependent microstimulation effects on *me* and z. Same format as in a).

c) Scatterplot of reward context-independent microstimulation effects on *me* and z. Same format as in a).

d) Graphical representation of the correlation patterns in among DDM parameters for reward asymmetry effects alone (left), reward context-dependent microstimulation effects (middle) and reward context-independent microstimulation effects (right). Lines between DDM parameter names indicate significant correlation ($p < 0.05$) in both monkeys.

e) Projections of "rew" (red), "rew-estim" (purple) and "estim" (green) effects on DDM parameters in a 3D space defined by the first three principal components derived from the "rew" effects. The same "rew" data were plotted in both panels. Note the tighter "rew-estim" cluster that parallels closer to the "rew" cluster, compared to the "estim" cluster.

f) Cumulative fractions of explained variance for the "rew" (red), "rew-estim" (purple) and "estim" (green) effects on DDM parameters, using principal components derived from the "rew" effects.

g) Hypothesized placement of caudate neurons (blue) in the decision process.

Extended Data Figure 1. Percentage of neurons showing significant non-zero linear regression coefficients for different regressors and task epochs.
Dashed lines indicate chance level. Blue shading: overlapping epochs between target onset and motion onset (400 ms window after target onset; window from target onset to motion onset; 400 ms window before motion onset) ; yellow shading: overlapping epochs during motion viewing (fixed window from motion onset to 100 ms before median saccade onset; variable window from motion onset to 100 ms before saccade onset for each trial); green shading: 300 ms perisaccade window starting at 100 ms before saccade onset; magenta shading: 400 ms postsaccade window.

Extended Data Figure 2.
a) Scatterplot of microstimulation effects on choice bias for the two reward contexts. Gray data points represent sessions without significant effect for either reward contexts.

b) Scatterplot of microstimulation effects on sensitivity for the two reward contexts. Same format as a.

c) Histogram of the difference in AIC between the full model, in which all DDM parameters were allowed to vary by reward context and microstimulation status, and a reduced model, in which all DDM parameters were allowed to vary by reward context but not microstimulation status. Negative AIC means that the full model is better.

Extended Data Figure 3. Histograms of DDM parameters.
Values were from the best model for each session. The top row ("Estim") shows reward context-independent microstimulation effects. The bottom row ("Rew x Estim") plots reward context-dependent microstimulation effects. Triangles indicate median values; red triangles indicate non-zero median values (Wilcoxon signed-rank test, $p < 0.05$).

Extended Data Figure 4. Visualization of microstimulation effect category and neural activity patterns.
a) Same scatterplot as Fig. 2d with category annotation of microstimulation effects on choice bias. The categories were: 1)increasing reward bias (contralateral bias in contralateral-large reward blocks, ipsilateral bias in ipsilateral-large reward blocks), 2) contralateral bias only in contralateral-large reward blocks, 3) contralateral bias only in ipsilateral-large reward blocks, 4) contralateral bias in both blocks but larger in contralateral-large reward blocks, 5) contralateral bias in both blocks but larger in ipsilateral-large reward blocks, 6) similar contralateral bias in both blocks, 7) ipsilateral bias in both blocks but larger in contralateral-large reward blocks, 8) ipsilateral bias in both blocks but larger in ipsilateral-large reward blocks, 9) ipsilateral bias only in contralateral-large reward blocks, 10) ipsilateral bias only in ipsilateral-large reward blocks, and 11) no significant microstimulation-induced bias for either reward contexts (not shown).

G) Same scatterplot as Fig. 2e with category annotation of microstimulation effects on sensitivity. The categories were: 1) decrease of sensitivity in contralateral-large reward blocks, decrease of sensitivity in ipsilateral-large reward blocks, 2) increase of sensitivity only in contralateral-large reward blocks, 3) increase of sensitivity only in ipsilateral-large reward blocks, 4) similar increase in sensitivity in both blocks, 5) decrease of sensitivity only in contralateral-large reward blocks, 6) decrease of sensitivity only in ipsilateral-large reward blocks, and 7) no significant effects for either reward blocks (not shown).

c) Visualization of neural modulation patterns for different categories of microstimulation effects on choice bias (a). Only sessions with significant microstimulation effects are included. For each session (columns), neural modulation is represented by the values of significant non-zero regression coefficients. Lower case letters (a,b,c) indicate the example sessions in Fig. 2.

d) Visualization of neural modulation patterns for different categories of microstimulation effects on sensitivity (b). Same format as c.

Extended Data Figure 5. Lack of relationship between certain microstimulation effects and neural modulation strength.

a-b) Scatterplot of the regression coefficient value for "RewSize" and the reward context-dependent microstimulation effect on *me* (a) and *z* (b).

c) Scatterplot of the regression coefficient value for "RewCont" and the reward context-dependent microstimulation effect on choice bias.

Extended Data Figure 6. Microstimulation effects showed similar dependencies on neural modulation strength in both monkeys.

a-d) Scatterplots of data from Monkey C. Similar format as Fig. 3. Red texts indicate *p* values for red data points. Black texts indicate *p* values for black data points.

e-h) Scatterplots of data from Monkey F. Lines/shading show results with $p<0.05$.

Extended Data Figure 7.

a-d) Cartoon illustration of anticipated microstimulation effects for different underlying mechanisms.

e-g) Graphical representation of the correlation patterns in among DDM parameters for all data pooled (e), only data from monkey C (f), and only data from monkey F (g). Lines indicate correlation with $p < 0.05$. Thick lines indicate correlation with $p < 0.01$.

h) Graphical representation of the correlation pattern common to both monkeys for the "base" adjustments.

Extended Data Figure 8. Scatterplots of effects on DDM parameters, for reward asymmetry effects ("rew"), reward context-dependent microstimulation effects ("rew x estim" and reward context-independent microstimulation effects ("estim"). Each panel used the same format as Fig. 4a. Numbers above each panel indicate the *p* values from linear regression. Data were pooled from both monkeys.

Extended Data Figure 9. Same format as Extended Data Figure 8. Data were from monkey C.

Extended Data Figure 10. Same format as Extended Data Figure 8. Data were from monkey F.

References

1. Redgrave, P., Prescott, T.J. & Gurney, K. The basal ganglia: a vertebrate solution to the selection problem? *Neuroscience* 89, 1009-1023 (1999).
2. Ding, L. & Gold, J.I. The basal ganglia's contributions to perceptual decision making. *Neuron* 79, 640-649 (2013).
3. Bogacz, R. & Gurney, K. The basal ganglia and cortex implement optimal decision making between alternative actions. *Neural Comput* 19, 442-477 (2007).
4. Lo, C.C. & Wang, X.J. Cortico-basal ganglia circuit mechanism for a decision threshold in reaction time tasks. *Nat Neurosci* 9, 956-963 (2006).
5. Wei, W., Rubin, J.E. & Wang, X.J. Role of the indirect pathway of the basal ganglia in perceptual decision making. *J Neurosci* 35, 4052-4064 (2015).
6. Barto, A.G. Adaptive critics and the basal ganglia. in *Models of information processing in the basal ganglia* (ed. J.C. Houk, J.L. Davis & D.G. Beiser) 215-232 (MIT Press, Cambridge, MA, 1995).
7. Mink, J.W. The basal ganglia: focused selection and inhibition of competing motor programs. *Progress in neurobiology* 50, 381-425 (1996).
8. Kable, J.W. & Glimcher, P.W. The neurobiology of decision: consensus and controversy. *Neuron* 63, 733-745 (2009).
9. Frank, M.J. Hold your horses: a dynamic computational role for the subthalamic nucleus in decision making. *Neural Netw* 19, 1120-1136 (2006).
10. Rao, R.P. Decision making under uncertainty: a neural model based on partially observable markov decision processes. *Frontiers in computational neuroscience* 4, 146 (2010).
11. Caballero, J.A., Humphries, M.D. & Gurney, K.N. A probabilistic, distributed, recursive mechanism for decision-making in the brain. *PLoS computational biology* 14, e1006033 (2018).
12. Ratcliff, R. & Frank, M.J. Reinforcement-based decision making in corticostriatal circuits: mutual constraints by neurocomputational and diffusion models. *Neural Comput* 24, 1186-1229 (2012).
13. Berns, G.S. & Sejnowski, T.J. How the basal ganglia make decisions. in *Neurobiology of Decision-Making* (ed. A.R. Damasio, H. Damasio & Y. Christen) 101-113 (Springer-Verlag, Berlin, 1995).
14. Kimchi, E.Y. & Laubach, M. Dynamic encoding of action selection by the medial striatum. *J Neurosci* 29, 3148-3159 (2009).
15. Cavanagh, J.F.*, et al.* Subthalamic nucleus stimulation reverses mediofrontal influence over decision threshold. *Nat Neurosci* 14, 1462-1467 (2011).
16. Hollerman, J.R., Tremblay, L. & Schultz, W. Involvement of basal ganglia and orbitofrontal cortex in goal-directed behavior. *Prog Brain Res* 126, 193-215 (2000).
17. Cai, X., Kim, S. & Lee, D. Heterogeneous coding of temporally discounted values in the dorsal and ventral striatum during intertemporal choice. *Neuron* 69, 170-182 (2011).
18. Hikosaka, O., Kim, H.F., Yasuda, M. & Yamamoto, S. Basal ganglia circuits for reward value-guided behavior. *Annu Rev Neurosci* 37, 289-306 (2014).
19. Samejima, K. & Doya, K. Multiple representations of belief states and action values in corticobasal ganglia loops. *Ann N Y Acad Sci* 1104, 213-228 (2007).
20. Santacruz, S.R., Rich, E.L., Wallis, J.D. & Carmena, J.M. Caudate Microstimulation Increases Value of Specific Choices. *Curr Biol* 27, 3375-3383 e3373 (2017).
21. Ding, L. & Gold, J.I. Caudate encodes multiple computations for perceptual decisions. *J Neurosci* 30, 15747-15759 (2010).
22. Ding, L. & Gold, J.I. Separate, causal roles of the caudate in saccadic choice and execution in a perceptual decision task. *Neuron* 75, 865-874 (2012).

23. Tai, L.H., Lee, A.M., Benavidez, N., Bonci, A. & Wilbrecht, L. Transient stimulation of distinct subpopulations of striatal neurons mimics changes in action value. *Nat Neurosci* 15, 1281-1289 (2012).
24. Yartsev, M.M., Hanks, T.D., Yoon, A.M. & Brody, C.D. Causal contribution and dynamical encoding in the striatum during evidence accumulation. *eLife* 7 (2018).
25. Wang, L., Rangarajan, K.V., Gerfen, C.R. & Krauzlis, R.J. Activation of Striatal Neurons Causes a Perceptual Decision Bias during Visual Change Detection in Mice. *Neuron* 97, 1369-1381 e1365 (2018).
26. Lau, B. & Glimcher, P.W. Value representations in the primate striatum during matching behavior. *Neuron* 58, 451-463 (2008).
27. Seo, M., Lee, E. & Averbeck, B.B. Action selection and action value in frontal-striatal circuits. *Neuron* 74, 947-960 (2012).
28. Summerfield, C. & Tsetsos, K. Building Bridges between Perceptual and Economic Decision-Making: Neural and Computational Mechanisms. *Front Neurosci* 6, 70 (2012).
29. Fan, Y., Gold, J.I. & Ding, L. Ongoing, rational calibration of reward-driven perceptual biases. *eLife* 7, e36018 (2018).
30. Lauwereyns, J., Watanabe, K., Coe, B. & Hikosaka, O. A neural correlate of response bias in monkey caudate nucleus. *Nature* 418, 413-417 (2002).
31. Hikosaka, O., Nakamura, K. & Nakahara, H. Basal ganglia orient eyes to reward. *J. Neurophysiol.* 95, 567-584 (2006).
32. Ding, L. & Gold, J.I. Neural correlates of perceptual decision making before, during, and after decision commitment in monkey frontal eye field. *Cereb Cortex* 22, 1052-1067 (2012).
33. Watanabe, M. & Munoz, D.P. Saccade suppression by electrical microstimulation in monkey caudate nucleus. *J Neurosci* 30, 2700-2709 (2010).
34. Watanabe, M. & Munoz, D.P. Saccade reaction times are influenced by caudate microstimulation following and prior to visual stimulus appearance. *J Cogn Neurosci* 23, 1794-1807 (2011).
35. Nakamura, K. & Hikosaka, O. Facilitation of saccadic eye movements by postsaccadic electrical stimulation in the primate caudate. *J Neurosci* 26, 12885-12895 (2006).
36. Zylberberg, A., Fetsch, C.R. & Shadlen, M.N. The influence of evidence volatility on choice, reaction time and confidence in a perceptual decision. *eLife* 5 (2016).

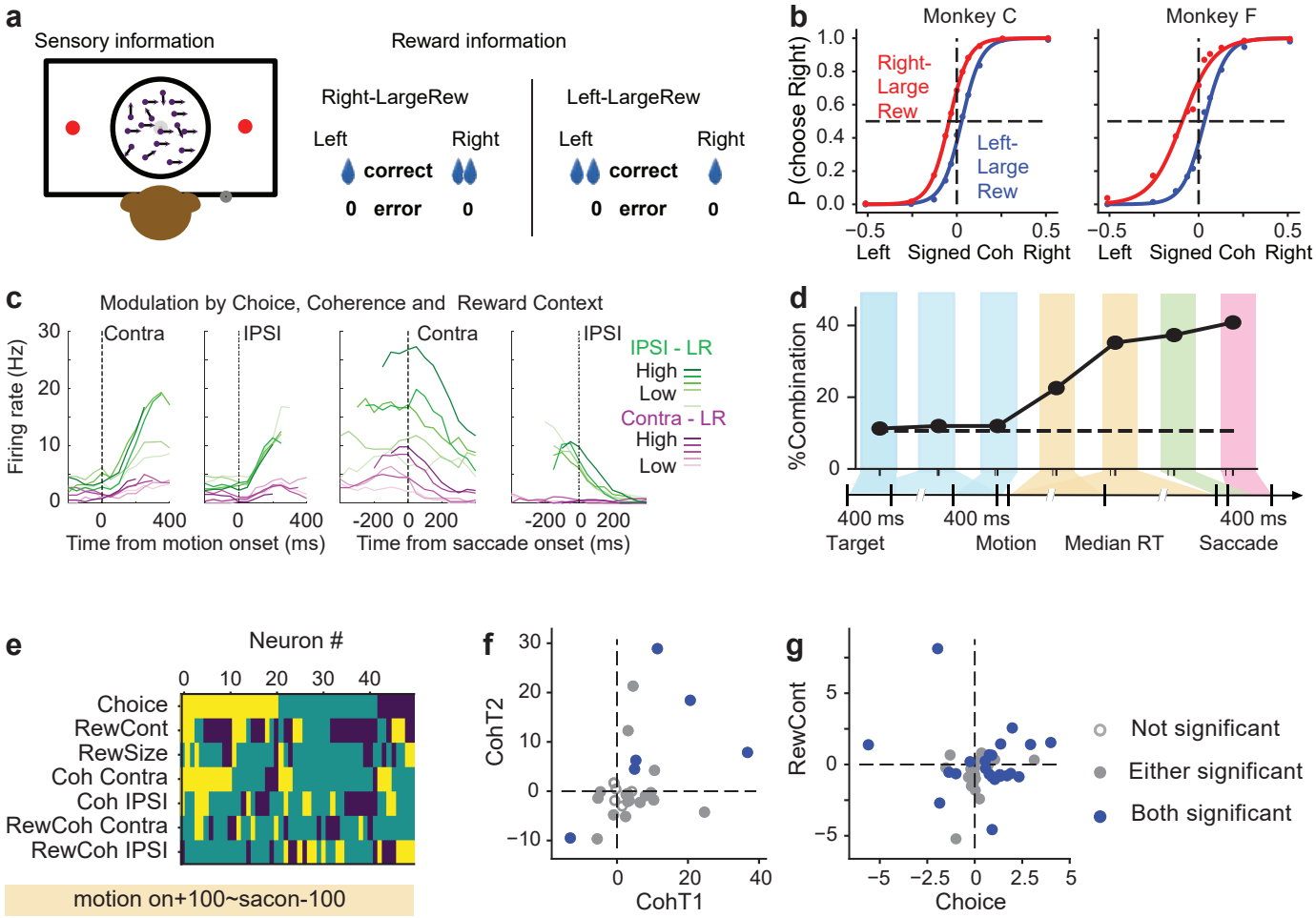

Figure 1. Task, behavior and caudate activity.

a) On the asymmetric reward motion discrimination task, a monkey observed the random-dot motion stimulus and reported the perceived global motion with a saccade to one of the two choice targets. Motion direction and strength (coherence) were pseudo-randomly selected from trial to trial. In a block of trials, correct rightward choice was paired with large reward and correct leftward choice was paired with small reward. Error trials were not rewarded. The asymmetric reward contexts were alternated between blocks of trials.

b) Average choice behavior of two monkeys (n = 17493 trials from 38 sessions for monkey C and 29599 trials from 79 sessions for monkey F). Note the gap between red and blue curves, which indicates that both monkeys were more likely to choose the choice paired with large reward.

c) Example neuron showing joint modulation by choice, motion strength and reward context. Colors indicate reward contexts; shading indicates the coherence level.

d) Percentage of neurons showing joint visual evidence and reward modulation. Dashed line indicates chance level.

e) Color map showing the presence of significant non-zero regression coefficients for each combination neuron (in rows). Yellow: positive; dark blue: negative; green: not significant; criterion: $p = 0.05$. Neurons were sorted by the signs of coefficients.

f) Scatterplot of regression coefficients for coherence for the two choices. Only combination neurons with significant choice selectivity were shown. Gray: neurons without significant coherence modulation; cyan: neurons with significant coherence modulation for only one choice; red: neurons with significant coherence modulation for both choices.

g) Scatterplot of regression coefficients for choice and reward context for combinations neurons with significant modulation by either during motion viewing. Cyan: neurons with significant modulation by either choice or reward context; red: neurons with significant modulation by both.

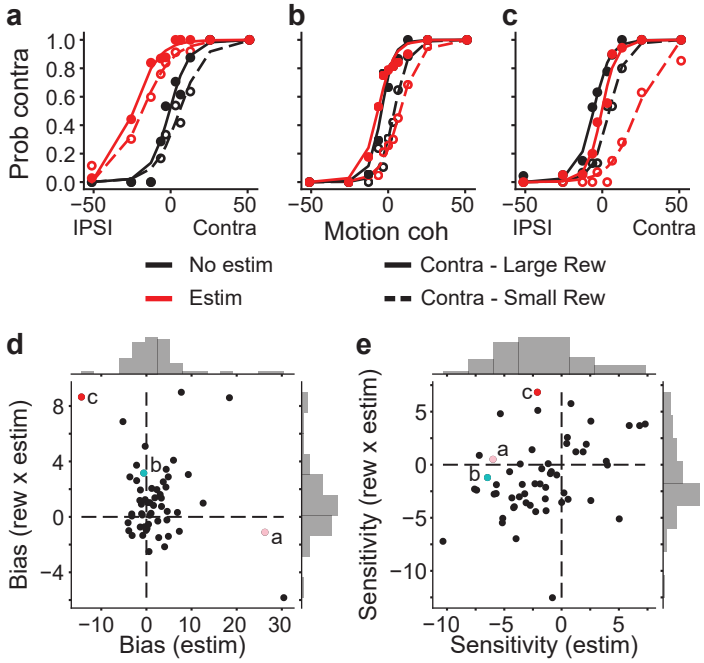

Figure 2. Caudate microstimulation affected monkeys' decision behavior.

a-c) Three example sessions from monkey C, showing different patterns of microstimulation effects.

d) Scatterplot of the fitted $bias_{estim}$ and $bias_{rew \times estim}$ terms in logistic function. Top panel: histogram of the fitted $bias_{estim}$ term (median 0.79% coherence, Wilcoxon signed rank test, $p = 0.015$). Right panel: histogram of the fitted $bias_{rew \times estim}$ term (median 0.83% coherence, $p = 0.0035$). Colored circles with labels (a, b, c) correspond to the example sessions in a-c.

e) Scatterplot of the fitted s_{estim} and $s_{rew \times estim}$ terms in logistic function. Top panel: histogram of the fitted s_{estim} term (median -2.1, $p = 0.0012$). Right panel: histogram of the fitted $s_{rew \times estim}$ term (median -1.8, , $p = 0.019$). Colored circles with labels (a, b, c) correspond to the example sessions in a-c.

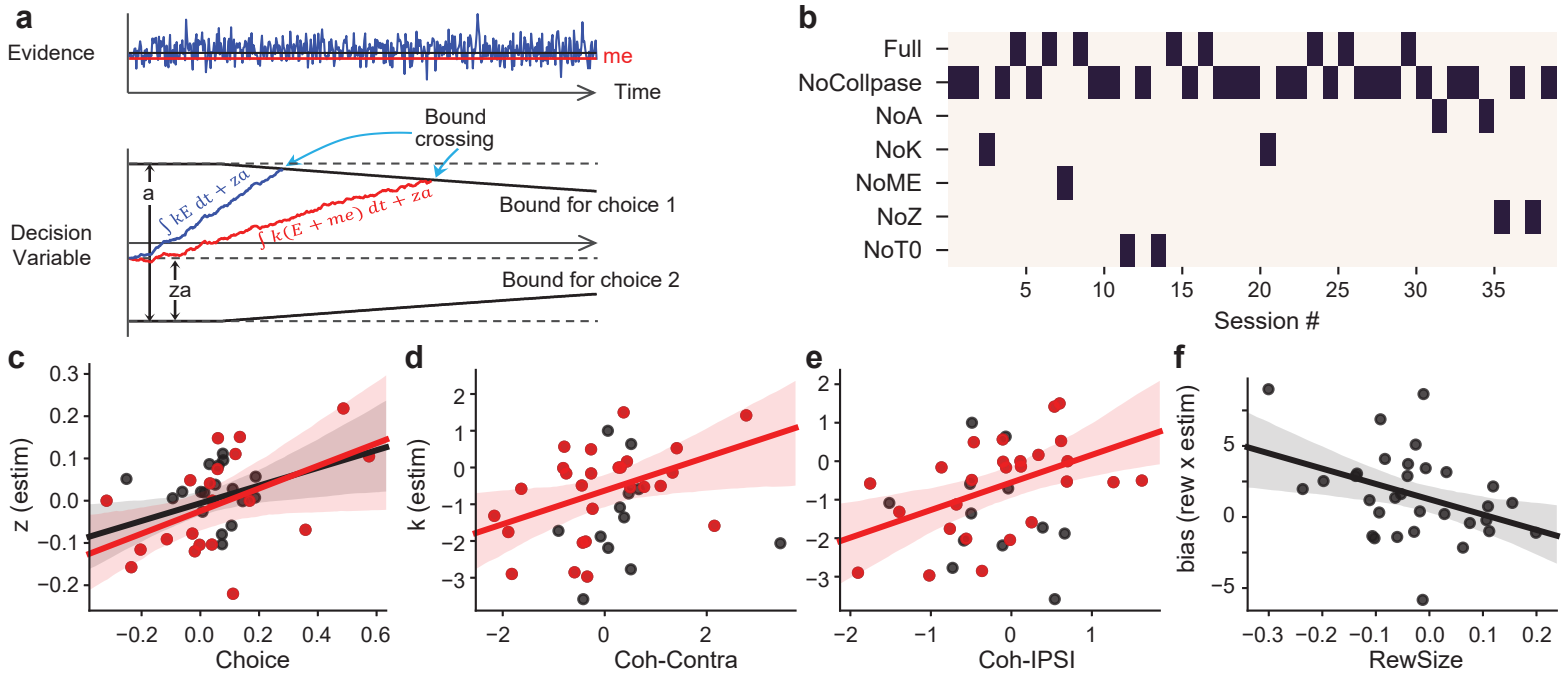

Figure 3. Microstimulation effects depended on neural modulation strength.

a) Drift-diffusion model. Motion evidence (E) is modeled as samples from a Gaussian distribution (mean = $k\times$ *signed coh*, var = 1). Decision variable is computed as the time integral of E and compared at each time point to two time-varying decision bounds. Crossing of either bound results in the corresponding choice. Reaction time is modeled as the sum of the time to bound-crossing and a non-decision time. See Methods for details.

b) Color map showing the best DDM variant for sessions with microstimulation effects, which was defined as showing a smaller AIC with the full model than a reduced model without microstimulation-induced changes (sessions to the left of the red arrow in Extended Data Fig. 2c).

c) Scatterplot of the regression coefficient value for "Choice" and the reward context-independent microstimulation effect on z. Black circles and line: all sessions. Red circles and line: sessions in which the choice and reward context preferences were congruent.

d-e) Scatterplot of the regression coefficient value for coherence for trials with contralateral (d) and ipsilateral choices (e) and the reward context-independent microstimulation effect on k. Black circles: all sessions. Red circles and line: sessions in which the two coefficients for Coh-Contra and Coh-IPSI had the same signs.

f) Scatterplot of the regression coefficient value for RewSize and the reward context-dependent microstimulation effect on choice bias. Only sessions with significant microstimulation effects on choice bias (for either reward context) was included.

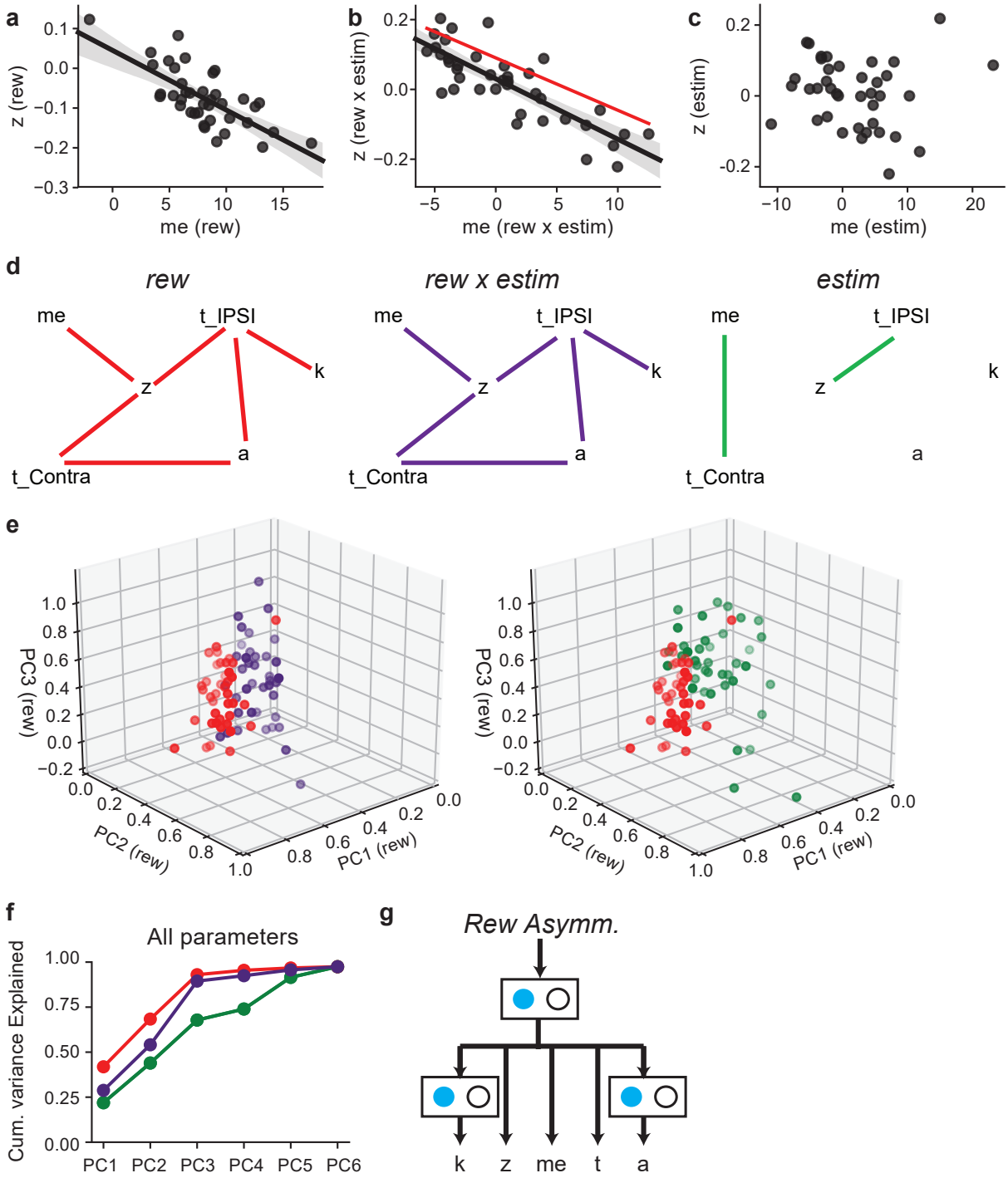

Figure 4. Correlated microstimulation effects on DDM parameters reflected correlated reward asymmetry effects.

a) Scatterplot of reward context modulation of *me* and *z* in the absence of microstimulation. The solid line indicates linear regression results with a significant, non-zero slope value. Shaded area indicates 95% confidence interval.

b) Scatterplot of reward context-dependent microstimulation effects on *me* and *z*. Same format as in a).

c) Scatterplot of reward context-independent microstimulation effects on *me* and *z*. Same format as in a).

d) Graphical representation of the correlation patterns in among DDM parameters for reward asymmetry effects alone (left), reward context-dependent microstimulation effects (middle) and reward context-independent microstimulation effects (right). Lines between DDM parameter names indicate significant correlation ($p < 0.05$) in both monkeys.

e) Projections of "rew" (red), "rew-estim" (purple) and "estim" (green) effects on DDM parameters in a 3D space defined by the first three principal components derived from the "rew" effects. The same "rew" data were plotted in both panels. Note the tighter "rew-estim" cluster that parallels closer to the "rew" cluster, compared to the "estim" cluster.

f) Cumulative fractions of explained variance for the "rew" (red), "rew-estim" (purple) and "estim" (green) effects on DDM parameters, using principal components derived from the "rew" effects.

g) Hypothesized placement of caudate neurons (blue) in the decision process.

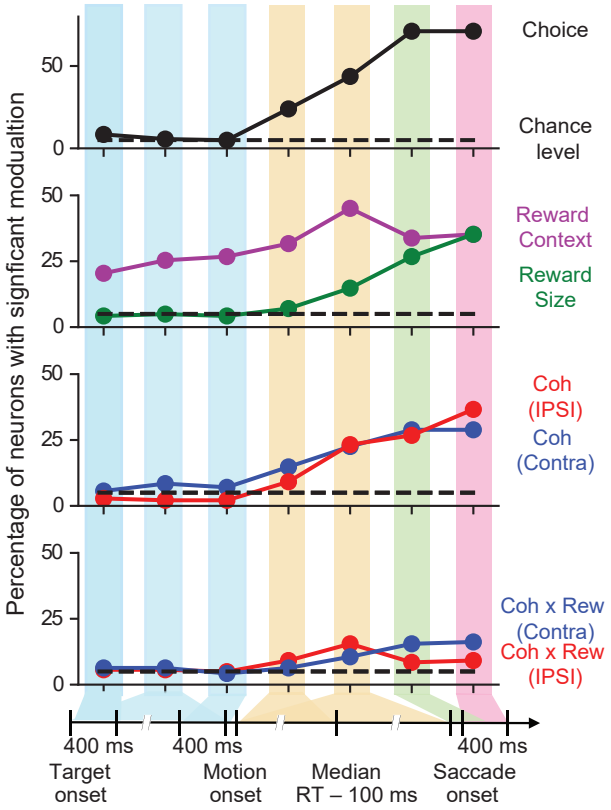

Extended Data Figure 1. Percentage of neurons showing significant non-zero linear regression coefficients for different regressors and task epochs.
Dashed lines indicate chance level. Blue shading: overlapping epochs between target onset and motion onset (400 ms window after target onset; window from target onset to motion onset; 400 ms window before motion onset) ; yellow shading: overlapping epochs during motion viewing (fixed window from motion onset to 100 ms before median saccade onset; variable window from motion onset to 100 ms before saccade onset for each trial); green shading: 300 ms perisaccade window starting at 100 ms before saccade onset; magenta shading: 400 ms postsaccade window.

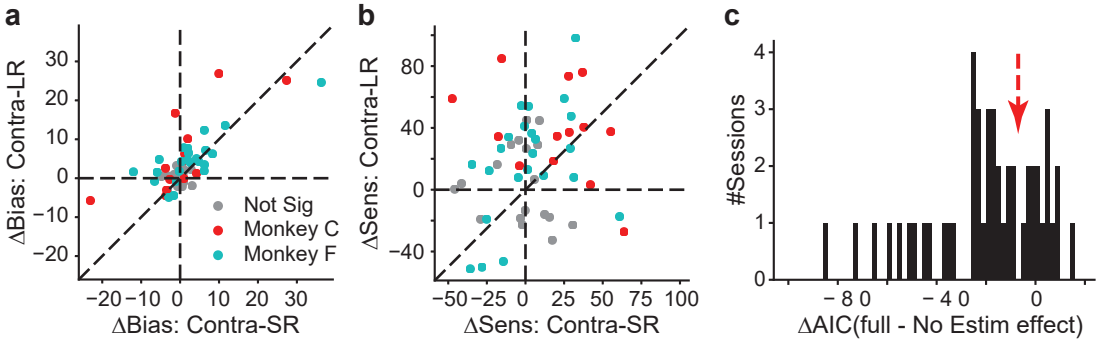

Extended Data Figure 2.
a) Scatterplot of microstimulation effects on choice bias for the two reward contexts. Gray data points represent sessions without significant effect for either reward contexts.

b) Scatterplot of microstimulation effects on sensitivity for the two reward contexts. Same format as a.

c) Histogram of the difference in AIC between the full model, in which all DDM parameters were allowed to vary by reward context and microstimulation status, and a reduced model, in which all DDM parameters were allowed to vary by reward context but not microstimulation status. Negative AIC means that the full model is better.

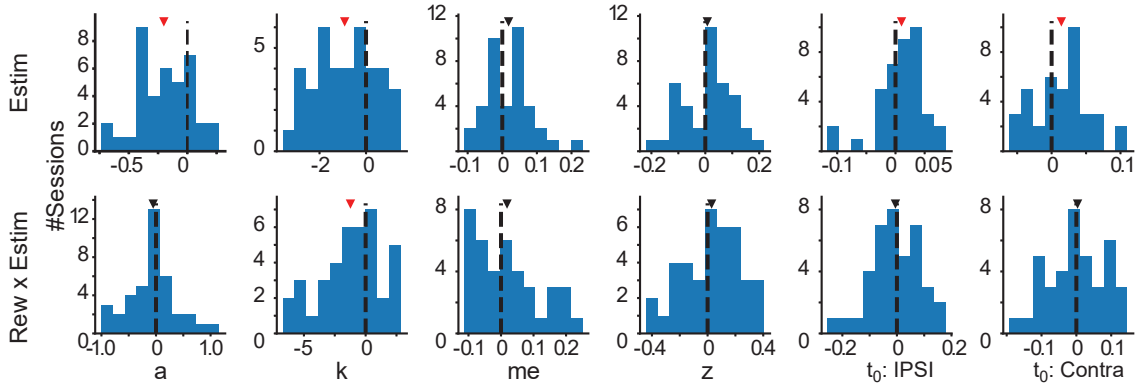

Extended Data Figure 3. Histograms of DDM parameters.
Values were from the best model for each session. The top row ("Estim") shows reward context-independent microstimulation effects. The bottom row ("Rew x Estim") plots reward context-dependent microstimulation effects. Triangles indicate median values; red triangles indicate non-zero median values (Wilcoxon signed-rank test, $p < 0.05$).

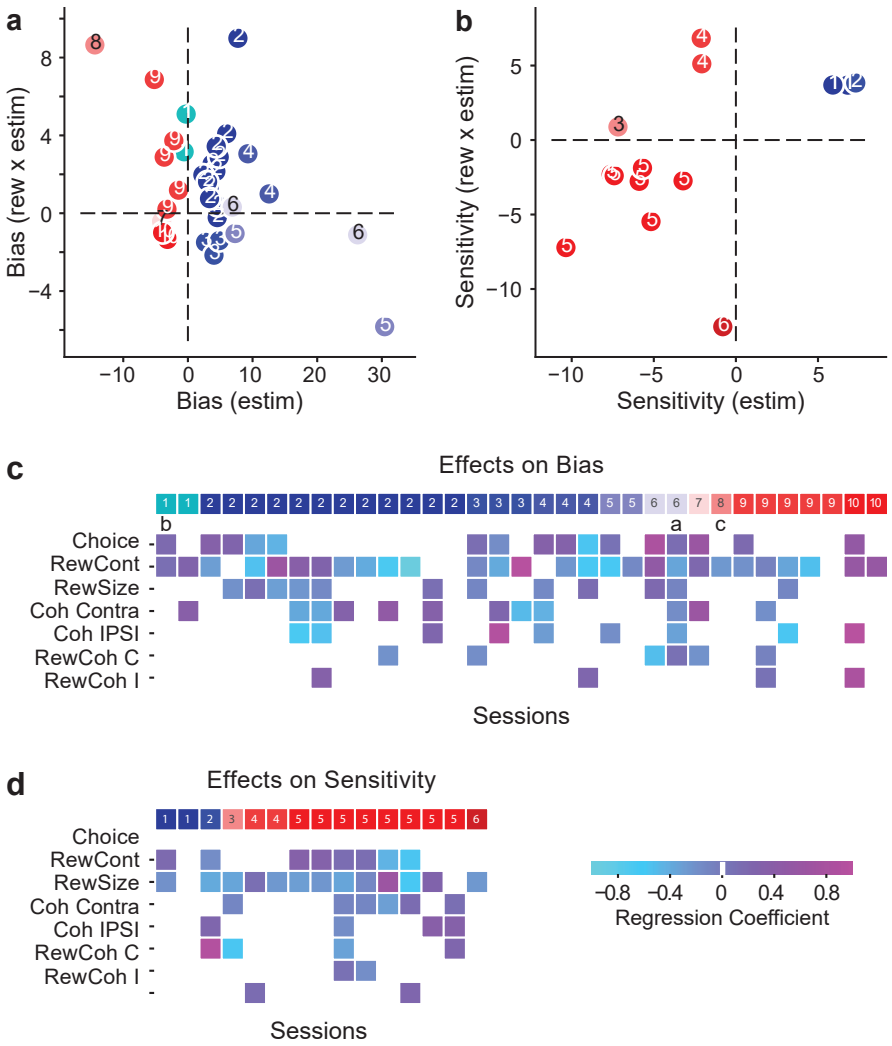

Extended Data Figure 4. Visualization of microstimulation effect category and neural activity patterns. a) Same scatterplot as Fig. 2d with category annotation of microstimulation effects on choice bias. The categories were: 1)increasing reward bias (contralateral bias in contralateral-large reward blocks, ipsilateral bias in ipsilateral-large reward blocks), 2) contralateral bias only in contralateral-large reward blocks, 3) contralateral bias only in ipsilateral-large reward blocks, 4) contralateral bias in both blocks but larger in contralateral-large reward blocks, 5) contralateral bias in both blocks but larger in ipsilateral-large reward blocks, 6) similar contralateral bias in both blocks, 7) ipsilateral bias in both blocks but larger in contralateral-large reward blocks, 8) ipsilateral bias in both blocks but larger in ipsilateral-large reward blocks, 9) ipsilateral bias only in contralateral-large reward blocks, 10) ipsilateral bias only in ipsilateral-large reward blocks, and 11) no significant microstimulation-induced bias for either reward contexts (not shown).

G) Same scatterplot as Fig. 2e with category annotation of microstimulation effects on sensitivity. The categories were: 1) decrease of sensitivity in contralateral-large reward blocks, decrease of sensitivity in ipsilateral-large reward blocks, 2) increase of sensitivity only in contralateral-large reward blocks, 3) increase of sensitivity only in ipsilateral-large reward blocks, 4) similar increase in sensitivity in both blocks, 5) decrease of sensitivity only in contralateral-large reward blocks, 6) decrease of sensitivity only in ipsilateral-large reward blocks, and 7) no significant effects for either reward blocks (not shown).

c) Visualization of neural modulation patterns for different categories of microstimulation effects on choice bias (a). Only sessions with significant microstimulation effects are included. For each session (columns), neural modulation is represented by the values of significant non-zero regression coefficients. Lower case letters (a,b,c) indicate the example sessions in Fig. 2.

d) Visualization of neural modulation patterns for different categories of microstimulation effects on sensitivity (b). Same format as c.

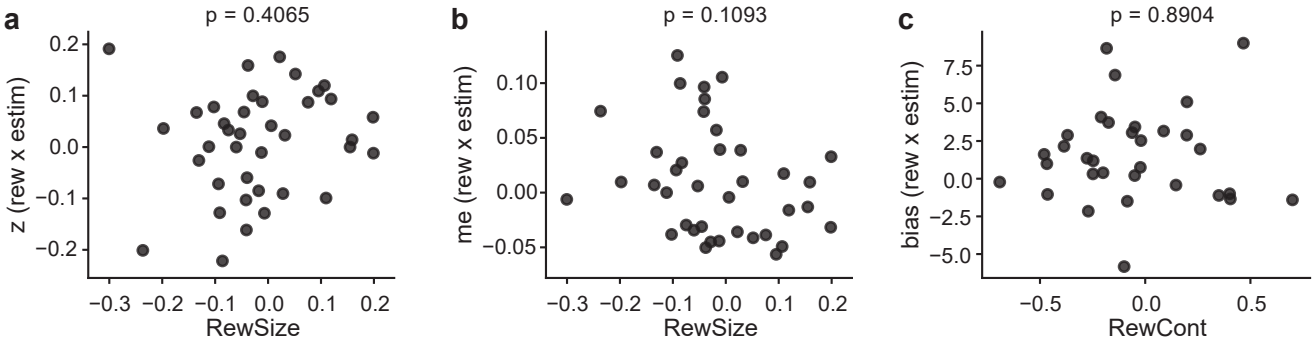

Extended Data Figure 5. Lack of relationship between certain microstimulation effects and neural modulation strength.

a-b) Scatterplot of the regression coefficient value for "RewSize" and the reward context-dependent microstimulation effect on *me* (a) and *z* (b).

c) Scatterplot of the regression coefficient value for "RewCont" and the reward context-dependent microstimulation effect on choice bias.

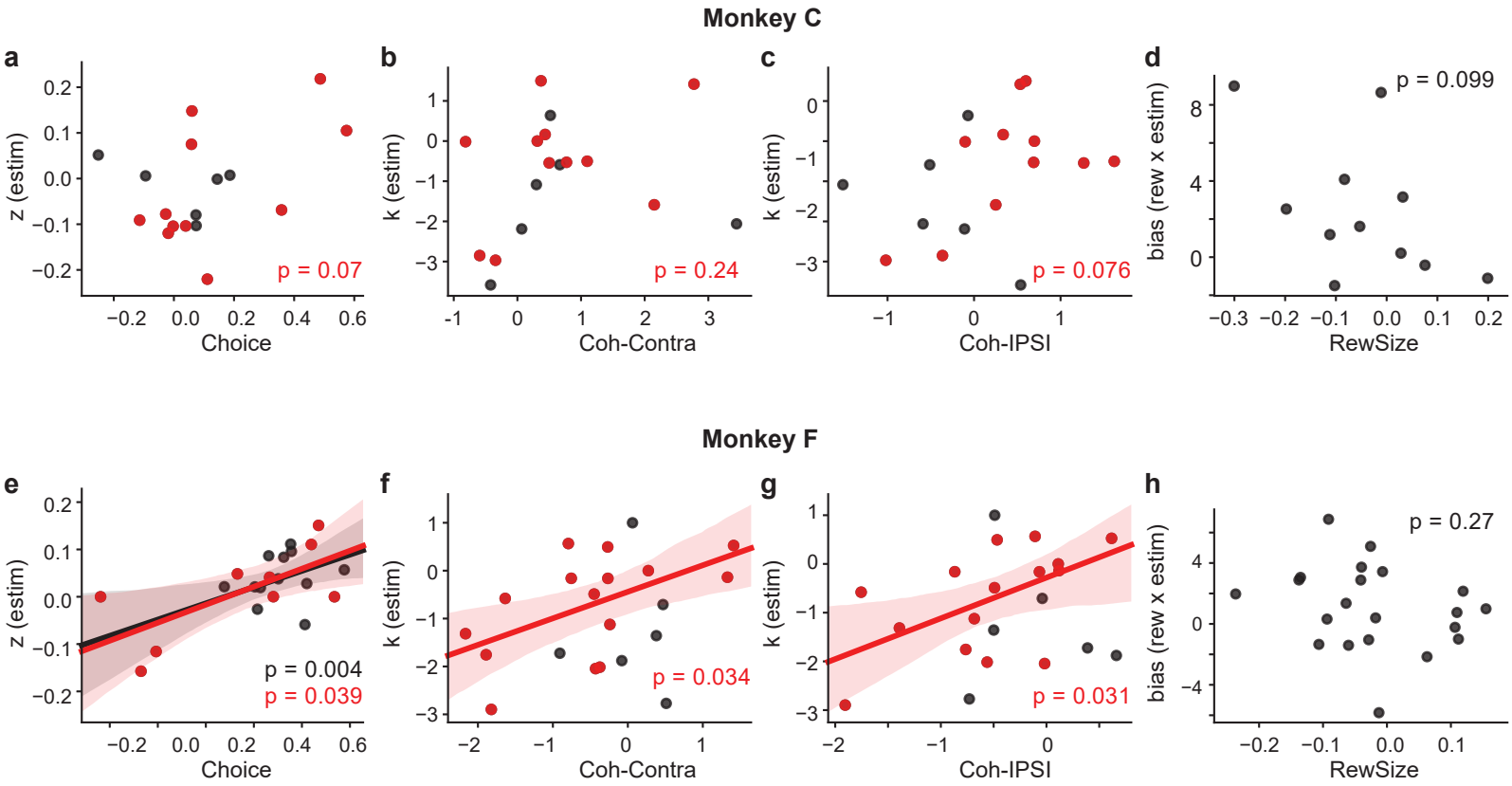

Extended Data Figure 6. Microstimulation effects showed similar dependencies on neural modulation strength in both monkeys.

a-d) Scatterplots of data from Monkey C. Similar format as Fig. 3. Red texts indicate *p* values for red data points. Black texts indicate *p* values for black data points.

e-h) Scatterplots of data from Monkey F. Lines/shading show results with $p<0.05$.

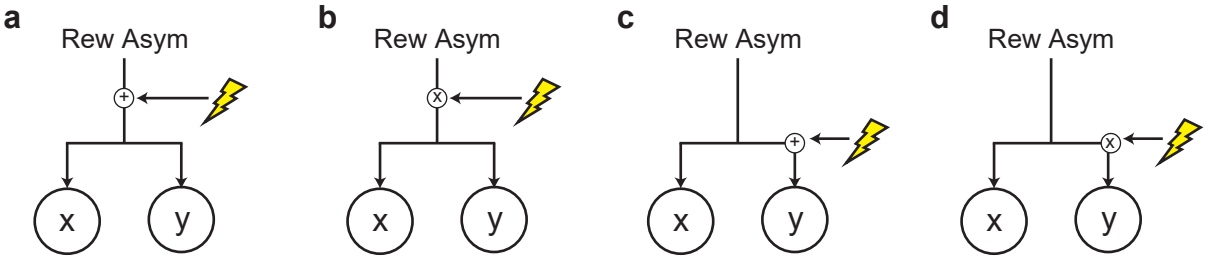

Expected effects	a	b	c	d
Correlated reward asymmetry effects (rew)	yes	yes	yes	yes
Reward context-dependent estim effects (rew x estim)	-	yes	-	yes for y
Reward context-independent estim effects (estim)	yes	-	yes for y	-
Correlated rew x estim effect, similar to rew	-	yes	-	-
Correlated estim effect, similar to rew	yes	-	-	-

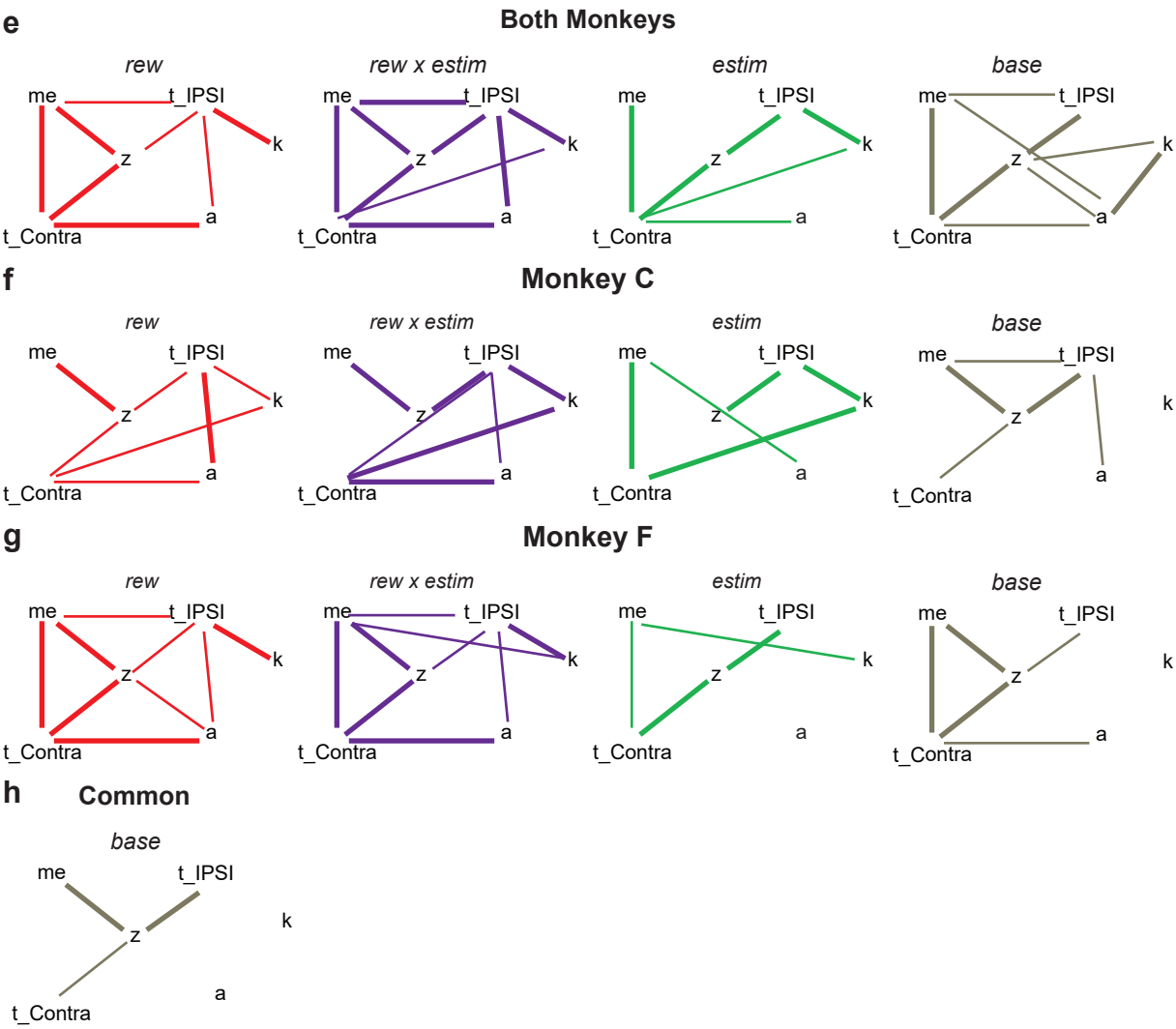

Extended Data Figure 7.
a-d) Cartoon illustration of anticipated microstimulation effects for different underlying mechanisms.
e-g) Graphical representation of the correlation patterns in among DDM parameters for all data pooled (e), only data from monkey C (f), and only data from monkey F (g). Lines indicate correlation with $p < 0.05$. Thick lines indicate correlation with $p < 0.01$.
h) Graphical representation of the correlation pattern common to both monkeys for the "base" adjustments.

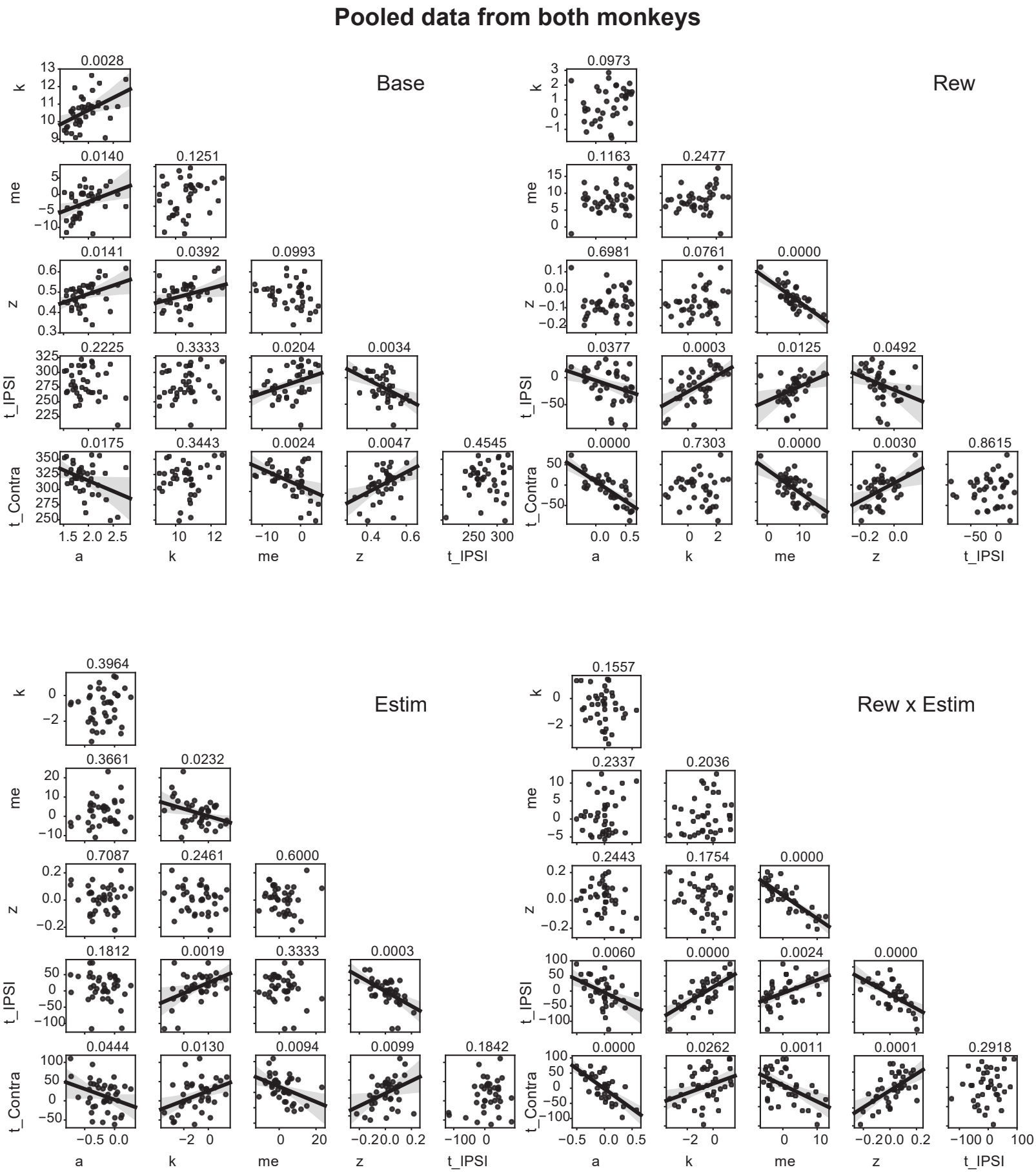

Extended Data Figure 8. Scatterplots of effects on DDM parameters, for reward asymmetry effects ("rew"), reward context-dependent microstimulation effects ("rew x estim" and reward context-independent microstimulation effects ("estim"). Each panel used the same format as Fig. 4a. Numbers above each panel indicate the *p* values from linear regression. Data were pooled from both monkeys.

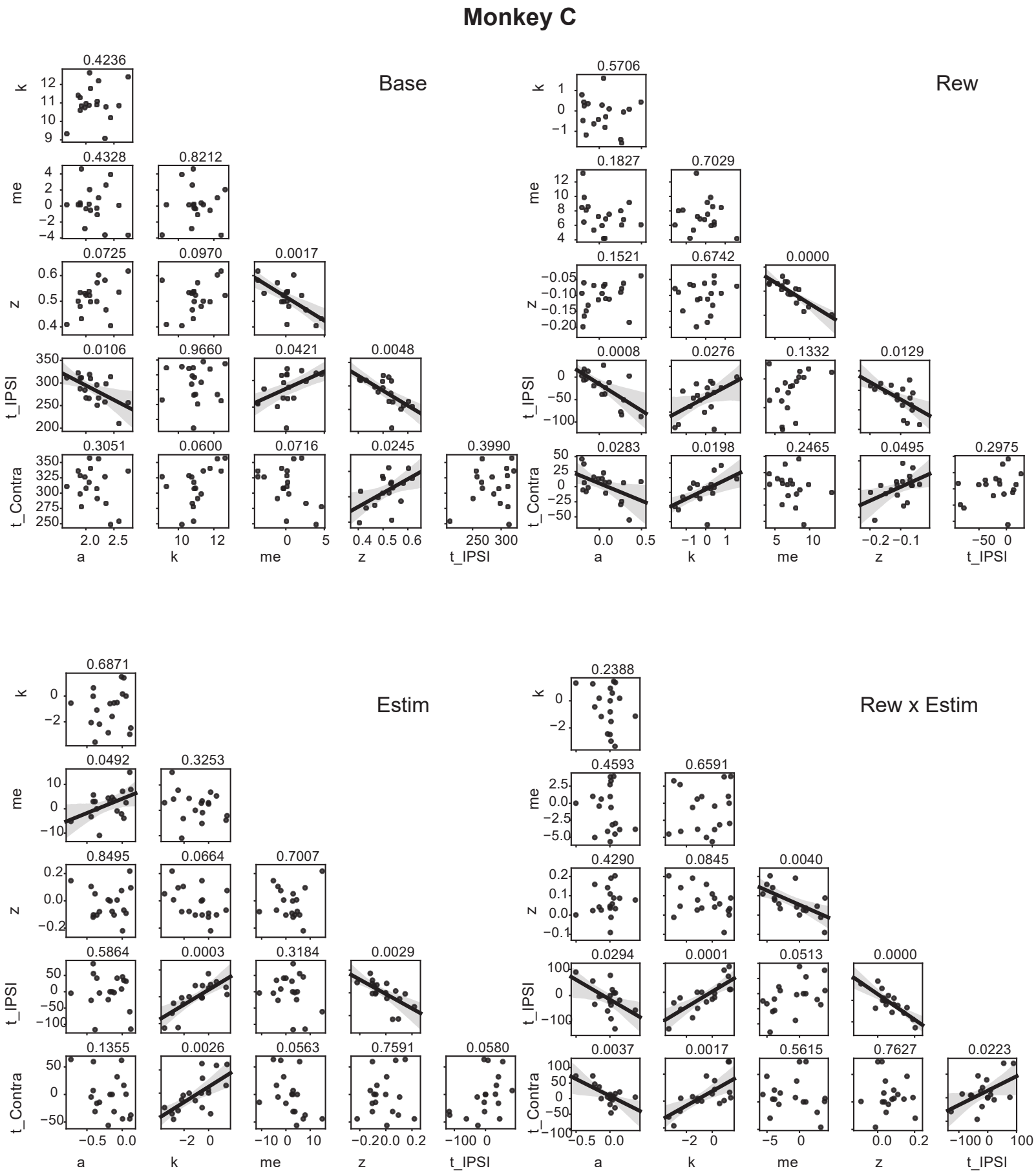

Extended Data Figure 9. Same format as Extended Data Figure 8. Data were from monkey C.

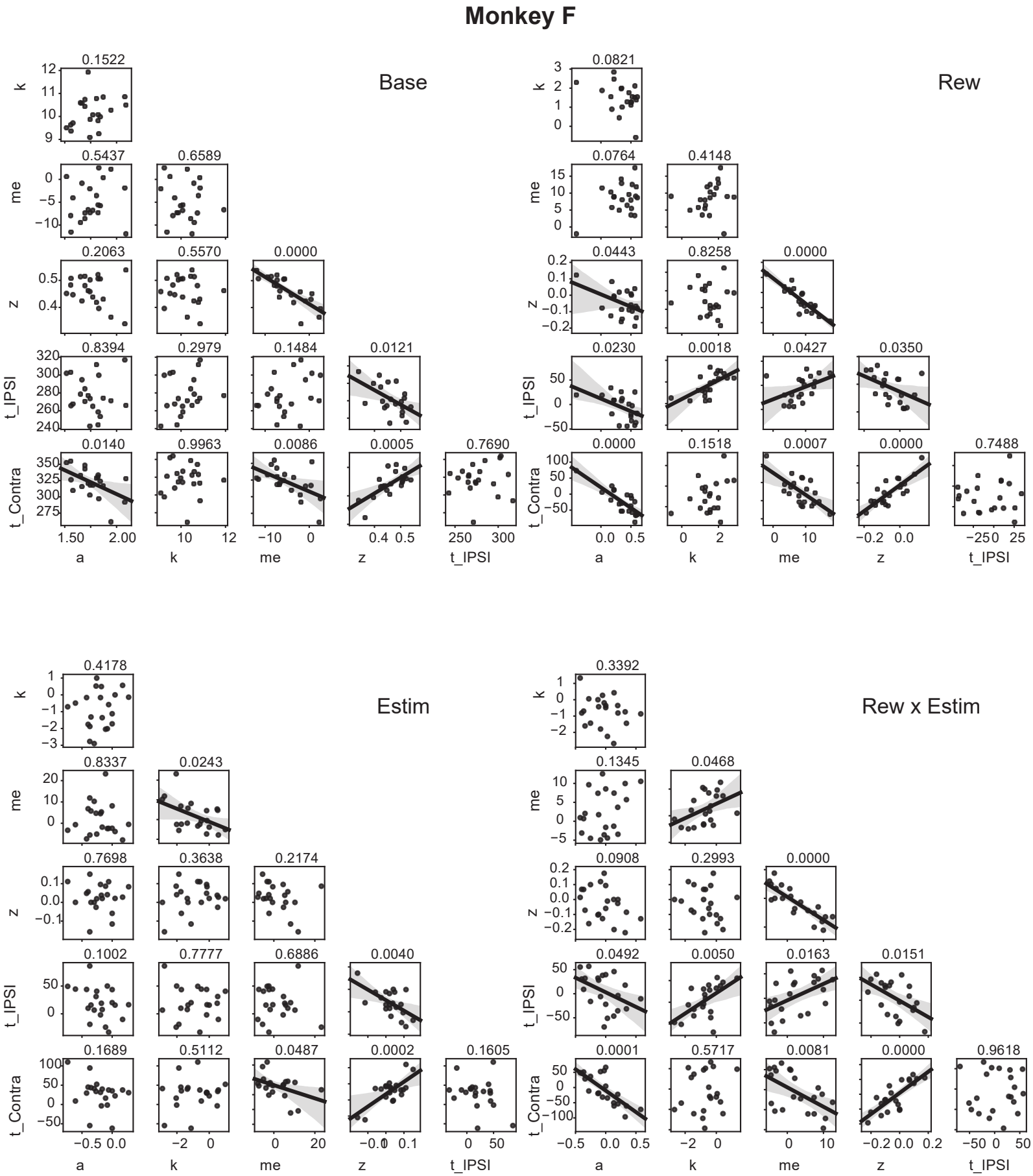

Extended Data Figure 10. Same format as Extended Data Figure 8. Data were from monkey F.